Water-Ethanol and Methanol-Ethanol Separations Using in Situ Confined Polymer Chains in a Metal-Organic Framework

Tang, Y.; Dubbeldam, D.; Tanase, S.

DOI
10.1021/acsami.9b14367

Publication date
2019

Document Version
Final published version

Published in
ACS Applied Materials and Interfaces

ACS APPLIED MATERIALS & INTERFACES

Research Article

Cite This: ACS Appl. Mater. Interfaces 2019, 11, 41383−41393

www.acsami.org

Water−Ethanol and Methanol−Ethanol Separations Using in Situ Confined Polymer Chains in a Metal−Organic Framework

Yiwen Tang, David Dubbeldam, and Stefania Tanase*

Van't Hoff Institute for Molecular Sciences, University of Amsterdam, Science Park 904, 1098 XH Amsterdam, The Netherlands

Supporting Information

ABSTRACT: This study presents a straightforward approach for the in situ polymerization of poly(*N*-isopropylacrylamide) (PNIPAM) chains within the one-dimensional (1D) pores of the five-coordinated zinc-based metal−organic framework DMOF in order to obtain new MOF-based composites. The loading amount of PNIPAM within DMOF ⊃ PNIPAM composites can be tuned by changing the initial weight ratio between NIPAM, which is the monomer of PNIPAM, and DMOF. The guest PNIPAM chains in the composites block partially the 1D pores of DMOF, thus leading to a narrowed nanospace. The water adsorption studies reveal that the water uptake increased by increasing the loading of PNIPAM in the final DMOF ⊃ PNIPAM composites, indicating that the exposed amide groups of PNIPAM gradually alter the hydrophobicity of pristine DMOF and lead to hydrophilic DMOF ⊃ PNIPAM composites. The composite with the highest loading of PNIPAM displays a selective adsorption for water and methanol over ethanol when using equimolar mixtures of methanol−ethanol and water−ethanol. This is confirmed by the single-component adsorption measurements as well as ideal adsorbed solution theory molecular simulations. Additionally, the water stability of pristine DMOF has been greatly improved after the incorporation of PNIPAM in its pores. PNIPAM can undergo a phase transition between hydrophobic and hydrophilic phases in response to a low temperature change. This property is used in order to control the desorption of water and methanol molecules, thus enabling an efficient and cost-effective regeneration process.

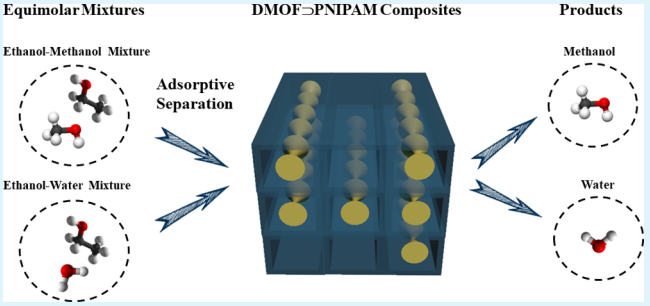

KEYWORDS: *in situ polymerization, PNIPAM, DMOF, composite, molecular separation*

1. INTRODUCTION

Bioethanol is foreseen to play a key role as an environmentally benign and renewable source of energy.[1] Currently, the raw product of bioethanol is a dilute mixture containing not only ethanol, but also impurities such as water and other organic alcohol byproducts. These impurities may reduce the conversion efficiency of bioethanol when used as fuel.[2,3] Thus, a process to remove impurities from the raw product of bioethanol until it reaches fuel-grade is necessary before further applications.[4] In industry, distillation technology is often used to remove impurities from the raw product of bioethanol, but the formation of azeotrope limits the purification of ethanol into fuel-grade and makes the entire process highly energy-intensive and inefficient.[5] Therefore, an energy-efficient adsorptive separation method has been proposed as an alternative approach.[6]

Metal−organic frameworks (MOFs) have demonstrated potential to be used as adsorbent materials for molecular storage and separations.[7,8] This is because of their high surface area, tunable size, and shape of the pores as well as their specific chemical functionality.[9,10] Not surprisingly, some MOFs are also utilized in the field of water−alcohol adsorptive separation.[3,11−14] There are two main strategies employed for the synthesis of MOFs used in water−alcohol adsorptive separations. One approach focuses on using organic linkers with specific functionalities to tune the hydrophobic or hydrophilic properties of the porous framework. For example, $\{[Dy(ox)(bpybc)(H_2O)](OH)\cdot 13H_2O\}_n$ is a charge-polarized MOF built from a zwitterionic organic linker, namely, 1,1′-bis(4-carboxybenzyl)-4,4′-bipyridinium dichloride (H_2bpybcCl_2).[3] This MOF separates water−alcohol mixtures based on the polarity difference between water and alcohol molecules.[3] ZIF-8 is a hydrophobic MOF constructed from Zn^{2+} ions and 2-methylimidazole (Hmim).[11] It selectively adsorbs alcohols through capillary condensation while repelling water molecules because of its high hydrophobicity.[11] The second approach utilizes flexible organic ligands because the flexibility of MOFs' structure can be inherited from the flexibility of the ligand. Such MOFs can undergo structural rearrangements in response to specific adsorbate molecules, leading to unconventional adsorption behavior due to the occurrence of breathing effects or gate-opening phenomenon.[15] $[Cu(mtpm)Cl_2]\cdot 20H_2O$,[12] TetZB,[13] and $[Zn_4(ox)_{1.5}]\cdot 4DMA\cdot 10DEF\cdot 10H_2O$[14] are such examples of flexible MOFs. These MOFs have water−alcohol adsorptive separation properties as a result of their flexible frameworks which

Received: August 12, 2019
Accepted: October 10, 2019
Published: October 10, 2019

require different energies to rearrange for water and alcohol molecules. However, there are two main challenges remaining in achieving efficient water−alcohol separation using MOFs. The first one is that most MOFs with potential in water−alcohol separations are not tested for their stability in the presence of water.[3,12−14] The second one is that none of the reported MOFs are prepared through a method that starts from a rational design of suitable pore sizes as well as tailor-made adsorptive affinity.

This study presents the synthetic design of a water stable MOF-based composite having the size of the pores and their functionality tailored specifically for the selective separation of water and methanol. Li et al.[16] reported that $[Zn_2(bdc)_2(DABCO)]$ (where H_2bdc = benzene-1,4-dicarboxylic acid and DABCO = 1,4-diazabicyclo[2.2.2.]octane), also known as DMOF, is suitable for the separation of water−alcohol mixtures because of its high hydrophobicity. Their studies have shown that water molecules are repelled by the hydrophobic pores whilst alcohol molecules are adsorbed through capillary condensation. Subsequent studies by Walton et al.[17] demonstrated that DMOF has very weak water stability as its crystal structure is completely changed after water adsorption thereby inhibiting its further application in water−alcohol separation processes. Therefore, it is very important to modify DMOF to improve its water stability while retaining its water−alcohol separation ability. DMOF has ordered one-dimensional (1D) pores (ca. 7.5 × 7.5 $Å^2$ along *c*-axis) which have smooth and flat walls.[18] These specific features allow the porous structure of DMOF to be tuned precisely at a nanoscale. Our goal was to directly narrow the size of DMOF's pores by incorporating organic polymers into its pores, in which the polymers can block partially the free volume available. This approach was inspired by the work of Uemura et al.,[9−22] which focused on the development of synthetic strategies to confine linear polymer chains in MOFs but they studied the thermal behavior of such composites. We aimed at designing DMOF−polymer composites with a pore size that enables the separation of water and alcohols based on the differences in their kinetic diameters. In this work, *N*-isopropylacrylamide (NIPAM), a monomer of poly(*N*-isopropylacrylamide) (PNIPAM) was chosen because it has amide groups that have high affinity for interaction with polar molecules, such as water and alcohols.[23] We hypothesized that the amide groups of the polymer will function as preferential adsorption sites for polar molecules, such as water, thus limiting their interaction with the DMOF framework. Moreover, PNIPAM is a thermo-responsive polymer. At temperatures below the lower critical solution temperature (LCST = 33 °C), PNIPAM is hydrophilic because the amide groups participate in hydrogen bonding interactions with polar molecules through hydrogen bonds. It exhibits hydrophobicity above LCST because of the breaking of the hydrogen bonds between the amide groups and the polar molecules.[24] Therefore, PNIPAM undergoes a structural phase transition from a linear to coil structure.[24] Related to water−alcohol adsorptive separations, we hypothesized that the thermo-responsive properties of the PNIPAM can be used to trigger the desorption of adsorbate molecules at lower temperature. This would enable lower energy costs in the regeneration process of the composite, thus increasing the energy efficiency of the process as compared with other adsorbent materials. For example, the zeolite Linde Type 4A requires a thermal treatment at 200−300 °C for the desorption of water molecules.[16]

To the best of our knowledge, there is only one study reporting on the use of polynaphthylene to block partially the pores of MOF-5 to achieve selective CO_2 capture.[25] Therefore, it is demonstrated here the general applicability of such approach for other MOF structures, which in turn enables the extension of the applicability range of the MOF−polymer composites. We discuss the synthesis and characterization of the composites obtained by confining the PNIPAM polymer in the 1D pores of DMOF as well as their water−alcohol separation properties studied experimentally and in terms of the grand-canonical Monte Carlo (GCMC) simulations.

2. EXPERIMENTAL SECTION

2.1. Materials and Methods. All chemicals and solvents were purchased from commercial suppliers and used without further purification. Infrared spectra (IR, 4000−400 cm^{-1}, resol, 0.5 cm^{-1}) were recorded on a Varian 660 FTIR spectrometer equipped with a GladiATR devise using KBr pellets as the transmission technique. Raman spectra were carried out using an Olympus BX51M upright microscope with excitation at 632.8 nm (Thorlabs HNL 120-1 HeNe laser) via a 50 times magnification objective with 10 mW at the sample. Raman scattering was collected and delivered to a Shamrock 163 spectrograph via a round to line fiber bundle and detected with an iDus-416 charge-coupled device detector. All the NMR spectra were recorded on a Bruker Advance 400 MHz NMR spectrometer and using DMSO-d_6 as the solvent. Powder X-ray diffraction (PXRD) measurements were carried out on a Rigaku Miniflex X-ray diffractometer. The measurements were done in the 5°−50° range using a Cu Kα source. Thermogravimetric analysis (TGA) and differential scanning calorimetry (DSC) measurements were carried out on a STA 449 F3 Jupiter (NETZSCH Instrument) unit. The measurements were performed in air (20 mL/min) at 35−800 or 80−175 °C with a heating rate of 5 or 2.0 °C/min, respectively. The morphology of the samples with sputtered gold was studied by using field-emission scanning electron microscopy (FESEM, FEI Verios 460 scanning electron microscope) operated at 5 kV. N_2 sorption isotherms were measured at 77 K on a Thermo Scientific Surfer. Water, methanol, and ethanol sorption experiments were performed in an isothermal Setaram Calvert 80 microcalorimeter, connected to a home built manometric apparatus.[26] The adsorption enthalpies of water, methanol, and ethanol were recorded simultaneously as a function of sorption uptakes.[26]

2.2. Synthesis of DMOF. DMOF was synthesized using a modification of a reported procedure.[27] Particularly, 0.5 g (1.68 mmol) of $Zn(NO_3)_2{\cdot}6H_2O$, 0.28 g (1.68 mmol) of H_2bdc, and 0.094 g (0.84 mmol) of DABCO were dissolved in 10 mL dimethylformamide (DMF) in a 20 mL Teflon-capped borosilicate tube. One drop of concentrated HNO_3 was additionally added per 10 mL of DMF. The tube was then sealed and heated in an oven at 120 °C for 24 h to obtain colorless crystals. The mother liquid of the as-synthesized crystals was exchanged with $CHCl_3$ and the procedure repeated to exchange the old solvent with fresh $CHCl_3$ every 8 h for 3 days. The colorless crystals were then collected by filtration and dried under ambient conditions. The collected product was further activated under vacuum ($<10^{-4}$ Torr) at 120 °C for 8 h prior to characterization measurements and its use in the composite synthesis.

2.3. Synthesis of PNIPAM. 0.55 g (4.86 mmol) of NIPAM monomer and 0.022 g (0.131 mmol) of radical initiator 2,2′-azobis(2-methylpropionitrile) (AIBN) were added in a 10 mL reaction tube under a nitrogen atmosphere. The mixture was then dissolved in 2 mL tetrahydrofuran (THF) and placed in an oil bath at 70 °C overnight. Then, the reaction mixture was cooled to room temperature and diethyl ether was slowly added in the above reaction mixture. The polymer formed as a white precipitate was filtered off and then redissolved in THF and reprecipitated with diethyl ether. The above process was repeated three times. The purified polymer was then

DOI: 10.1021/acsami.9b14367
ACS Appl. Mater. Interfaces 2019, 11, 41383−41393

dried under reduced pressure at room temperature and further activated under vacuum (<10^{-4} Torr) at 60 °C for 8 h prior to the following measurements.

2.4. Synthesis of the DMOF ⊃ PNIPAM Composites. Composites of type DMOF ⊃ PNIPAM were obtained by in situ polymerization of the NIPAM monomer using the activated DMOF. In order to fully introduce the monomer and radical initiator into the channels of DMOF, the 0.1 g activated DMOF was immersed in a THF solution (1 mL) containing the NIPAM monomer and AIBN initiator (4.0 wt % to the monomer NIPAM) under a nitrogen atmosphere for 2 h. Typical weight ratios of NIPAM to DMOF were as follows: DMOF ⊃ PNIPAM-**1**, 0.25; DMOF ⊃ PNIPAM-**2**, 0.60; DMOF ⊃ PNIPAM-**3**, 0.90. The excess of THF was completely removed by evaporation under vacuum at room temperature. The resulting white powder was heated in an oil bath at 70 °C overnight to conduct the polymerization, yielding the composites of type DMOF ⊃ PNIPAM-**1**, **2**, and **3**, respectively. The as-synthesized DMOF ⊃ PNIPAM composites were washed several times with fresh methanol to remove the surface bulk polymer PNIPAM, then the composites were activated under vacuum (<10^{-4} Torr) at 60 °C for 8 h prior to the following measurements.

2.5. GCMC Simulation. The adsorption computations of single-components were performed using the configurational-bias Monte Carlo algorithm in the grand-canonical ensemble. The systems were modeled in full atomistic detail using calibrated classical force fields. Periodic boundary conditions were used to extrapolate the finite system results to macroscopic bulk values. The simulation was run with 300 000 cycles after an initialization run of 150 000 cycles. In each cycle and on each molecule, a Monte Carlo move was attempted consisting of a random choice from moves like translation, rotation, reinsertion, and insertion/deletion of molecules. A DMOF cell of 21.98 × 21.98 × 38.63 Å^3 was used using an interaction cutoff of 11.99 Å. The Ewald-summation with a relative precision of 10^{-6} was used to model charge interactions. The force field was TraPPE for methanol and ethanol and Tip5pEw for water, respectively. The adsorbate−framework interactions were modeled using the DREIDING force field.

3. RESULTS AND DISCUSSION

3.1. Synthesis and Characterization. The in situ formation of PNIPAM polymer chains within the 1D pores of DMOF is expected to narrow the pore size of DMOF to an appropriate size that enables the adsorption of smaller molecules from water−alcohol mixtures. This approach is summarized in Scheme 1.

In situ polymerization of the NIPAM monomer with different amounts within 1D pores of DMOF was performed at 70 °C using AIBN as the initiator. This led to composites of type DMOF ⊃ PNIPAM with different PNIPAM compositions. Figure 1 shows the PXRD patterns of DMOF, DMOF ⊃ PNIPAM-**1**, **2**, and **3**. It clearly indicates that the original crystal structure of the as-synthesized DMOF is retained in all the composites. Several main peaks are shifted slighter to lower 2θ values because of the changes in the geometry of the bdc^{2-} ligand, thus leading to an increase in the distance between the two neighboring Zn_2 units. This is a commonly observed feature of the activated DMOF.[18] Figure 2 reveals that the size and morphology of the DMOF ⊃ PNIPAM composite and DMOF crystals (all the DMOFs in this work refers to the activated DMOF from here forward) are almost the same. It confirms that the DMOF crystals were not influenced by the activation and polymerization procedures. Moreover, the SEM analysis also shows that there is no PNIPAM at the surface of the DMOF crystals (see Figure 2c−e).

The presence of the PNIPAM chains in the DMOF ⊃ PNIPAM composites was confirmed by FTIR and micro-

Scheme 1. (a,b) Schematic Illustration of the Linear PNIPAM Chain and DMOF; (c) Confinement of the Linear PNIPAM Chains in the 1D Pores of DMOF; (d) Adsorptive Water−Ethanol Separation on the Basis of Molecular Size

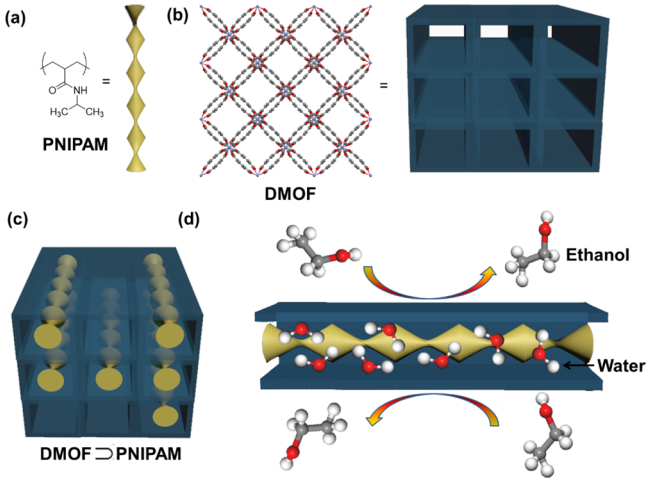

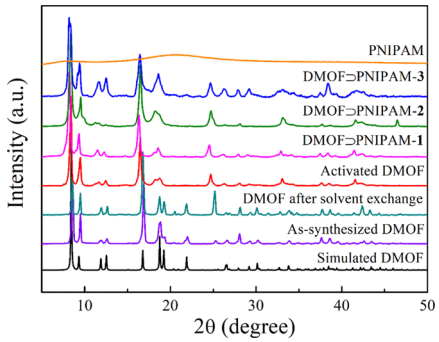

Figure 1. PXRD patterns of the as-synthesized DMOF, DMOF after solvent exchange, activated DMOF, the composites DMOF ⊃ PNIPAM-**1**, **2**, and **3** and PNIPAM. These patterns are compared with the simulated PXRD pattern of DMOF using the single-crystal crystallographic data.

Raman spectroscopic analysis. The FTIR spectra of the DMOF ⊃ PNIPAM composites show the characteristic peaks of both DMOF and PNIPAM (see Figure S1 in Supporting Information). Specifically, the bands at 1650 and 1380 cm^{-1} are assigned to the $\nu_{C=O}$ and ν_{C-O} stretching vibrations of the carboxylate groups of the bdc^{2-} ligands[28] whilst the bands at 1055, 820, and 750 cm^{-1} are assigned to the N−C−N deformation of DABCO.[28] Furthermore, the bands at 1650, 1554, and 1380 cm^{-1} correspond to the $\nu_{C=O}$ stretching vibration, ν_{C-N} stretching vibration, and the methyl bending vibration of amide I, amide II, and methyl group of PNIPAM, respectively.[29] Micro-Raman spectroscopy was further used for DMOF, PNIPAM, and DMOF ⊃ PNIPAM-**2** composite, respectively (see Figure 3). The DMOF ⊃ PNIPAM-**2** composite was selected here because it has a theoretical median PNIPAM concentration among the three composites. Several main peaks in the range of 860−1800 cm^{-1} of the DMOF ⊃ PNIPAM-**2** composite are assigned to the vibration modes of the bdc^{2-} and DABCO ligands, revealing the presence of DMOF.[30] Additionally, the band at about 1450 and 1160 cm^{-1} in the spectrum of the DMOF ⊃ PNIPAM-**2** composite can be ascribed to the C−N−C bending and ν_{C-Nazo} stretching vibration of PNIPAM.[31] Another broad

DOI: 10.1021/acsami.9b14367
ACS Appl. Mater. Interfaces 2019, 11, 41383−41393

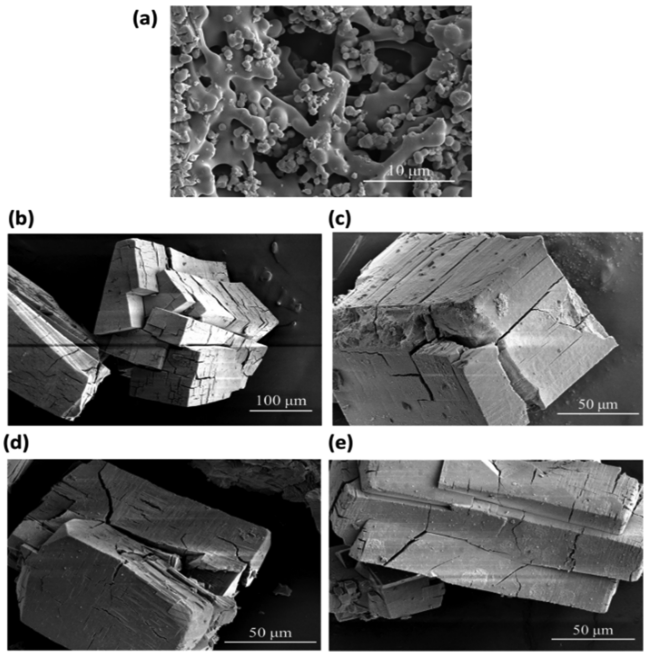

Figure 2. (a) SEM images of PNIPAM, (b) DMOF crystals and (c–e) DMOF ⊃ PNIPAM-**1**, **2**, and **3**, respectively.

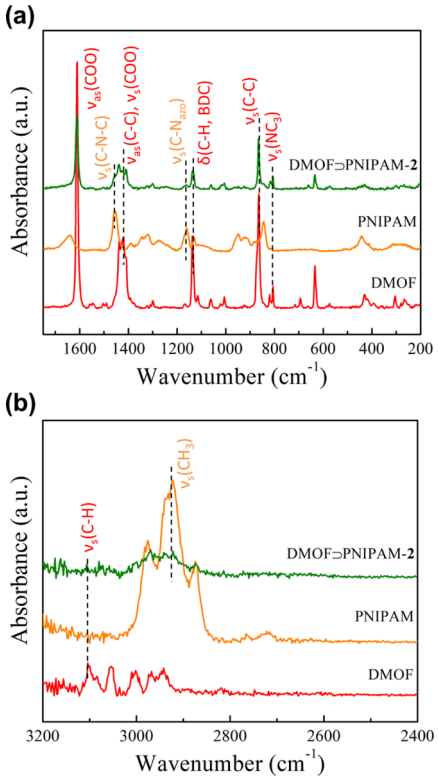

Figure 3. Raman spectra of the DMOF, PNIPAM, and DMOF ⊃ PNIPAM-**2** composite, respectively, in the range of (a) 200–1750 and (b) 2400–3200 cm^{-1}.

band is observed in the range of 2870–2970 cm^{-1} and it corresponds to the methyl stretching modes of PNIPAM.[31] Combined FTIR and Raman spectroscopic analysis indicates that the DMOF ⊃ PNIPAM composite contains both DMOF and PNIPAM.

The presence of PNIPAM polymer in DMOF is further confirmed by ^{1}H NMR studies. Because DMOF is insoluble in DMSO, no peaks from the organic ligands can be detected (see Figure S2 in Supporting Information). The ^{1}H NMR spectra of PNIPAM, DMOF ⊃ PNIPAM-**1**, **2**, and **3** composites show the same signals (see Figures 4, S3–S5 in Supporting

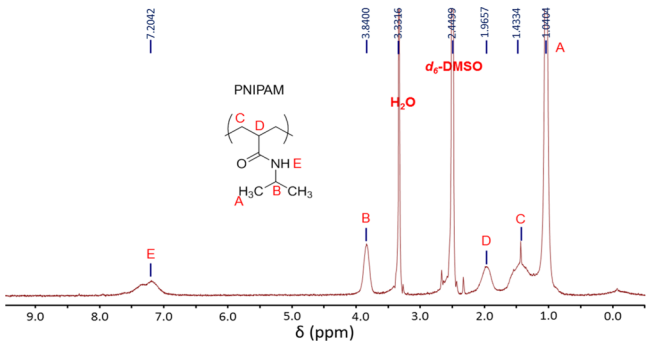

Figure 4. ^{1}H NMR spectrum of the DMOF ⊃ PNIPAM-**2** composite in DMSO-d_6 at ambient temperature.

Information). The characteristic signals at around δ = 1.0 and 4.0 ppm correspond to the methyl protons of the isopropyl groups and methyl protons of PNIPAM, respectively.[23] The broad signal in the range δ = 6.5–7.5 ppm is ascribed to the protons of the amide group and also of the PNIPAM chains.[23] Consequently, these results strongly suggest the presence of the PNIPAM polymer within the composites.

The PNIPAM undergoes an endothermic phase transition at a specific temperature which is known as glass transition temperature (T_g).[32] This phase transition includes a series of segmental motions and rotations in the surrounding free volume of PNIPAM.[32] Therefore, confining the PNIPAM chains within nanopores may reduce its free motion and rotation, thereby resulting in a change of the T_g. The DSC allows the identifcation of phase transition and the T_g of PNIPAM in DMOF ⊃ PNIPAM composites, and therefore, it can be used to shed light on the confinement of PNIPAM chains within the DMOF's pores. Figure 5 reveals the endothermic peak of PNIPAM at 135 °C, in agreement with the earlier studies.[33] The DSC curve of DMOF does not show any thermal effect in the temperature range from 80 to 190 °C. The DMOF ⊃ PNIPAM-**1**, **2**, and **3** composites show a phase transition at about 140, 160, and 180 °C, respectively, indicated by the endothermic peak observed in DSC. The

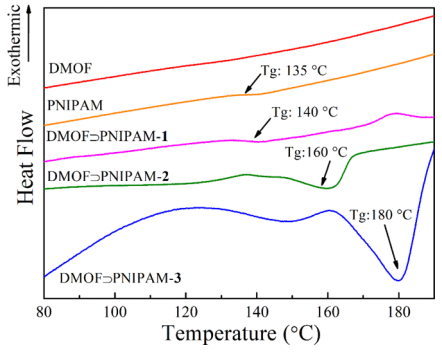

Figure 5. DSC heating curves of DMOF, PNIPAM, DMOF ⊃ PNIPAM-**1**, DMOF ⊃ PNIPAM-**2**, and DMOF ⊃ PNIPAM-**3** composites, respectively.

DOI: 10.1021/acsami.9b14367
ACS Appl. Mater. Interfaces 2019, 11, 41383–41393

shift of the T_g to higher values suggests that the PNIPAM chains are confined within the 1D pores of DMOF, thus needing more energy to undergo motion and rotation. This is because the 1D pores of DMOF limit the free volume required by PNIPAM to undergo segmental motion and rotation. Furthermore, the T_g of DMOF ⊃ PNIPAM composites increased by increasing the amount of PNIPAM. This is because the more PNIPAM is confined in the 1D pores of DMOF, the stronger is the intermolecular interactions between DMOF and PNIPAM chains. These interactions are established between the hydrophobic pore walls of DMOF and the alkane chains of PNIPAM. Therefore, a higher transition energy is needed for the composite with higher loading of PNIPAM. Such interactions were proposed earlier for the alkane polymers encapsulated in MOFs.[34,35]

The loading of PNIPAM in DMOF ⊃ PNIPAM-**1**, **2**, and **3** was determined using combined TGA and elemental analysis. Figure 6 shows that after solvent exchange, DMOF has a first

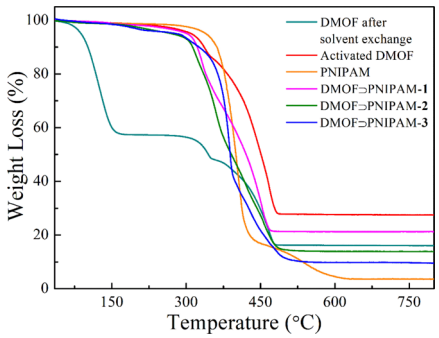

Figure 6. TGA curves of DMOF after solvent exchange, activated DMOF, PNIPAM, and DMOF ⊃ PNIPAM-**1**, DMOF ⊃ PNIPAM-**2** as well as DMOF ⊃ PNIPAM-**3** composites, respectively.

weight loss of about 62% below 150 °C which indicates the removal of all the guest $CHCl_3$ molecules. A subsequent weight loss occurs above 300 °C, corresponding to the framework decomposition. Activated DMOF does not contain any solvent molecule (see Figure 6), indicating that the empty 1D pores of DMOF can be used for in situ PNIPAM polymerization.

The depolymerization of PNIPAM polymer occurs above 350 °C, a temperature higher than the decomposition temperature of DMOF. Therefore, it is not possible to separate the depolymerization of PNIPAM from the decomposition of DMOF based on TGA. Nevertheless, because the TGA curves of all composite materials are very similar below 300 °C, the different residual weight percentage of composites corresponds to the different loadings of PNIPAM in the composites. Consequently, one can conclude that a higher loading of PNIPAM in composites leads to a lower residual weight percentage in the DMOF ⊃ PNIPAM composites. The elemental analysis was used as a complementary method to TGA to quantify the PNIPAM loading. The PNIPAM loading equals to 3.1, 12.8, and 15.0 wt %, respectively, for the DMOF ⊃ PNIPAM-**1**, **2**, and **3** composites (see Table S1 in Supporting Information). These results indicate that the loading of PNIPAM can be controlled by adjusting the weight ratio of monomer NIPAM to host DMOF before the polymerization reaction.

Nitrogen sorption studies were performed to determine the porosity of all materials and to further confirm the confinement of PNIPAM within DMOF's pores (see Figure 7). In agreement with earlier studies, DMOF has very high

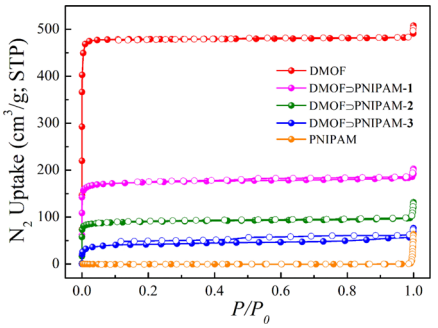

Figure 7. The N_2 sorption isotherms of the DMOF, PNIPAM, DMOF ⊃ PNIPAM-**1**, DMOF ⊃ PNIPAM-**2**, and DMOF ⊃ PNIPAM-**3** composites at 77 K, respectively. Solid and open symbols refer to adsorption and desorption, respectively.

Brunauer–Emmett–Teller (BET) and Langmuir surface areas of 1780 and 2090 m^2 g^{-1}, respectively.[16] In sharp contrast, the N_2 uptake is almost negligible for the PNIPAM polymer (less than 5 cm^3 g^{-1} at STP), confirming that it is a nonporous material. For the DMOF ⊃ PNIPAM composites (Figure 7), a decreasing of N_2 uptake can be observed with increasing the loading of PNIPAM. The corresponding BET and Langmuir surface areas of DMOF ⊃ PNIPAM-**1**, **2**, and **3** are 660/760, 340/390, and 160/180 m^2 g^{-1}, respectively. Nonlocal density functional theory (NLDFT) was used to calculate the pore size distributions (see Figure 8). Interestingly, with increasing the loading of PNIPAM, the pores with widths in the range of 7.5–8.6 Å (DMOF pores) gradually diminish whereas pores with widths in the range of

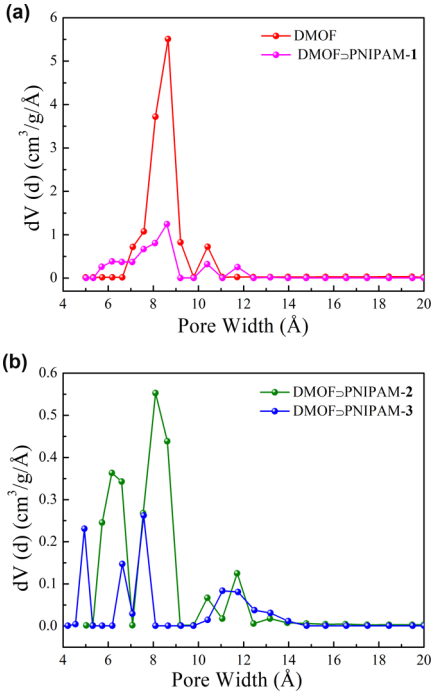

Figure 8. Pore size distribution plots of DMOF, DMOF ⊃ PNIPAM-**1**, DMOF ⊃ PNIPAM-**2**, and DMOF ⊃ PNIPAM-**3** composites calculated based on the N_2 adsorption isotherm measured at 77 K and using the NLDFT model.

DOI: 10.1021/acsami.9b14367
ACS Appl. Mater. Interfaces 2019, 11, 41383–41393

5.0−6.6 Å (DMOF ⊃ PNIPAM composite pores) emerge and gradually boost. The decreasing of the pore size of the DMOF ⊃ PNIPAM composites confirms the confinement of PNIPAM chains within the pores of DMOF.

3.2. Adsorption Studies. Taking into account the successful synthesis of the DMOF ⊃ PNIPAM composites with different PNIPAM loadings, further studies aimed at verifying the potential of these materials for size-driven adsorptive separations. Water−alcohol adsorptive separations were considered as model studies given the pore size of these composites as well as the presence of amide groups along PNIPAM chains suitable for adsorbing polar molecules.

Figure 9 shows the single sorption isotherms of DMOF for water, methanol, and ethanol at 30 °C. Note that DMOF is a

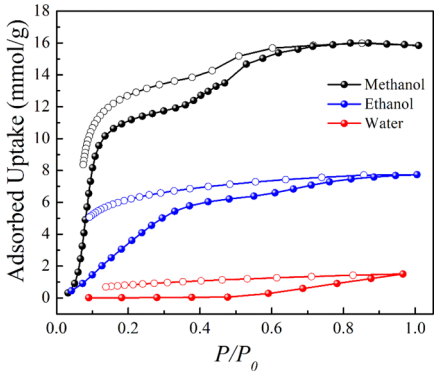

Figure 9. The sorption isotherms of DMOF for water, methanol, and ethanol at 30 °C, respectively. Solid and open symbols refer to adsorption and desorption, respectively.

material with high hydrophobicity because of the presence of hydrophobic bdc^{2-} and DABCO ligands.[36] Therefore, the interaction between DMOF and hydrophilic molecules is expected to be very weak. Such behaviour is revealed by the water adsorption isotherm of DMOF which is of type III, with a low water uptake of 1.5 mmol/g at P/P_0 = 0.98 (P_0 = 4 kPa at 30 °C).[36] For the case of methanol and ethanol adsorption, DMOF shows similar S-shaped adsorption isotherms. An initial adsorption plateau at P/P_0 < 0.1 (P_0 = 21 and 10 kPa at 30 °C for methanol and ethanol, respectively) indicate that the hydrophobic surface of DMOF has weak interaction with methanol and ethanol molecules. With increasing pressure, the uptake of methanol and ethanol rises sharply and finally reaches 16 and 7.7 mmol/g at P/P_0 = 0.98, respectively. This drastic enhance of methanol and ethanol uptake is because of the capillary condensation.[16] The molecular capillary condensation is usually dominated by entropic factors at high pressures. Therefore, the higher adsorption uptake of methanol than ethanol can be assigned to more efficient packing of the smaller methanol molecules (kinetic diameter is 3.6 Å) than ethanol molecules (kinetic diameter is 4.3 Å) within the 1D pores of DMOF.[37] A clear hysteresis loop can be observed for water, methanol, and ethanol sorption isotherms, indicating the occurrence of chemisorption between DMOF and the adsorbate molecules. For the water isotherm, the presence of the hysteresis can be ascribed to the interaction of water molecules with the Zn^{2+} ions in DMOF, which leads to the displacement of the coordinated ligand DABCO.[36] For both the methanol and ethanol isotherms, the presence of hysteresis is due to capillary condensation.[16,38]

Interestingly, the water adsorption behavior of DMOF ⊃ PNIPAM composites is much different than that of DMOF for which no initial plateau exists in the pressure range of 0 < P/P_0 < 0.5 (see Figure 10). This phenomenon reveals that the

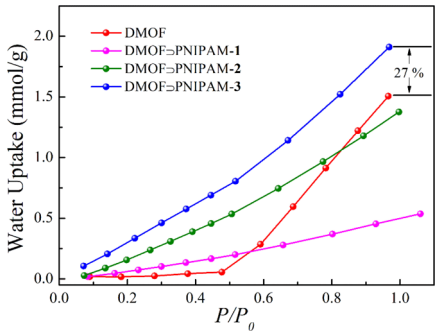

Figure 10. Water adsorption isotherms of DMOF, DMOF ⊃ PNIPAM-**1**, DMOF ⊃ PNIPAM-**2**, and DMOF ⊃ PNIPAM-**3** composites at 30 °C, respectively.

composites show a relative higher affinity for water than that of DMOF. The water uptakes of 0.5, 1.4, and 1.9 mmol/g are finally obtained for DMOF ⊃ PNIPAM-**1**, **2**, and **3** at P/P_0 = 0.98, respectively (see Figure 10). The fact that the water uptake increased by increasing the loading of PNIPAM in composites can be attributed to the increasing number of polar amide groups of PNIPAM in composites, favoring the water adsorption via hydrogen bonding.[39] The water uptake of DMOF ⊃ PNIPAM-**3** has increased considerably (ca. 27%) as compared with that of DMOF (1.5 mmol/g at P/P_0 = 0.98 and 30 °C). This is because DMOF ⊃ PNIPAM-**3** has the highest loading of amide groups among the three composites synthesized, thus leading to a significant decrease in the hydrophobicity of DMOF. The measured water adsorption enthalpies further confirm that the hydrophobicity of DMOF decreased with the increasing of PNIPAM loading in composites. The water adsorption enthalpies equal to −88, −127, −148, and −159 kJ/mol, for the initial water uptakes of DMOF, DMOF ⊃ PNIPAM-**1**, **2**, and **3**, respectively. It shows that the initial adsorption enthalpies are very high for the DMOF ⊃ PNIPAM composites. A high initial water adsorption enthalpy is also observed for other hydrophilic MOFs, for example, MIL-101Cr-NH_2 (~170 kJ/mol),[40] MIL-100 (Fe) (~100 kJ/mol),[41] H_2N-UiO-66 (~105 kJ/mol),[42] and NH_2-MIL-125 (~95 kJ/mol).[42,43] These values indicate that the water adsorption occurs first at the hydrophilic sites, such as the amide groups of the polymer, and then water clusters are formed around the adsorbed water molecules.[41,44] At higher water uptakes, all enthalpies decreased to about −43.6 kJ/mol, which is the enthalpy of evaporation of water (see Figure S6 in Supporting Information).[45] Additionally, the water adsorption enthalpy of DMOF ⊃ PNIPAM-**3** is the highest among DMOF and the other two composites in the entire pressure range. The results confirm that the interaction between water molecules and adsorbent materials increased by increasing the number of exposed amide groups in DMOF. Therefore, even though the DMOF ⊃ PNIPAM-**3** composite has the smallest surface area, because of the highest loading of amide groups from PNIPAM, it leads to the strongest affinity for water molecules and highest water uptake among the composites.

DOI: 10.1021/acsami.9b14367
ACS Appl. Mater. Interfaces 2019, 11, 41383−41393

DMOF ⊃ PNIPAM-3 composite was further selected to study its adsorption behavior for methanol and ethanol at 30 °C. This is because it displays the highest water uptake and the smallest pore size distribution among the three composites, which may lead to selective adsorption of the smaller water and methanol molecules over ethanol. As expected, the ethanol uptake of the DMOF ⊃ PNIPAM-3 composite is less than 1.1 mmol/g, which is much lower than that of DMOF under the same conditions (30 °C and P/P_0 = 0.98; see Figure 11). It is

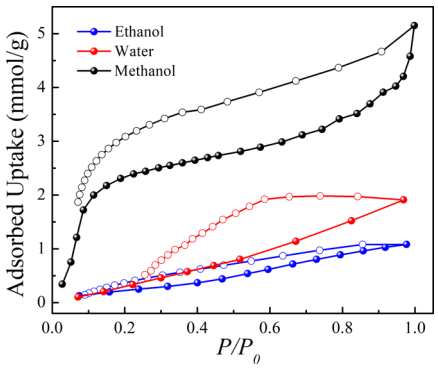

Figure 11. The sorption isotherms of water, methanol, and ethanol for the DMOF ⊃ PNIPAM-3 composite at 30 °C. Solid and open symbols refer to adsorption and desorption, respectively.

worth noting that the pore size distribution of DMOF ⊃ PNIPAM-3 (5−6.1 Å, see Figure 8) already indicates that the ethanol molecules may not be adsorbed because of their larger kinetic diameter (4.5 Å). Moreover, the smaller surface area of DMOF ⊃ PNIPAM-3 also contributes to the low ethanol adsorption uptake. The methanol adsorption isotherm of DMOF ⊃ PNIPAM-3 is different than that of DMOF, showing a methanol adsorption isotherm without the initial plateau (below P/P_0 = 0.1). This is because the amide groups of confined PNIPAM show affinity for methanol molecules through hydrogen bonding, similar to water adsorption. The measured methanol adsorption enthalpies for DMOF and DMOF ⊃ PNIPAM-3 composites at initial uptakes are −45 and −62 kJ/mol, respectively (see Figure S7 in Supporting Information). This confirms that the DMOF ⊃ PNIPAM-3 composite interacts strongly with methanol molecules as compared with pristine DMOF. The methanol uptake of DMOF ⊃ PNIPAM-3 is 4.3 mmol/g (30 °C and P/P_0 = 0.98), much lower than that observed for DMOF, even though its pore size is large enough for selective methanol adsorption (the kinetic diameter of methanol is 3.6 Å). However, this is expected because the surface area of DMOF ⊃ PNIPAM-3 is much lower than that of DMOF. The occurrence of the hysteresis loop confirms the presence of hydrogen bonding between the adsorbed molecules and the amide groups of the DMOF ⊃ PNIPAM-3 composite.

The GCMC molecular simulations were used to further shed light on the adsorption behavior of DMOF and DMOF ⊃ PNIPAM composites. Figure 12 shows the simulated adsorption behaviors of both DMOF and DMOF ⊃ PNIPAM-3 for water, methanol and ethanol, respectively. In the limit of low pressure, the fugacity equals pressure because the fugacity coefficient is unity. Therefore, we used the adsorption uptake as a function of fugacity to simulate the adsorption behavior.[46] Figure 12a shows that the simulated water isotherm of DMOF resembles type III adsorption behavior which is consistent with the experimental result, thus confirming the highly hydrophobic surface of DMOF.[47] The simulated methanol and ethanol isotherms show an adsorption behavior of type V, also in good agreement with the experimental results. It indicates that the hydrophobic DMOF has weak affinity for both methanol and ethanol in the initial pressure range and the alcohol uptake increased by

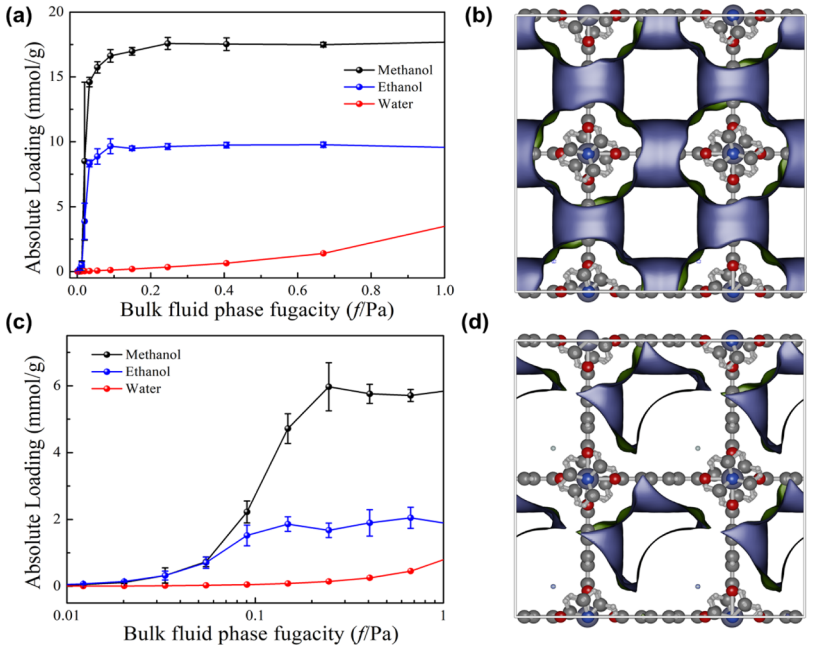

Figure 12. (a) Simulated adsorption isotherms of methanol, ethanol, and water in DMOF at 30 °C. (b) Possible adsorption surface of DMOF on the *ab* plane, shown in purple color. (c) Simulated adsorption isotherms for methanol, ethanol, and water of the DMOF ⊃ PNIPAM composite at 30 °C. (d) Possible adsorption surface of the DMOF ⊃ PNIPAM composite on the *ab* plane, shown in purple color. The artificial atomic centers are used to mimic the polymer PNIPAM chains, which are located at the bottom-right corner of 1D pores of DMOF.

DOI: 10.1021/acsami.9b14367
ACS Appl. Mater. Interfaces 2019, 11, 41383−41393

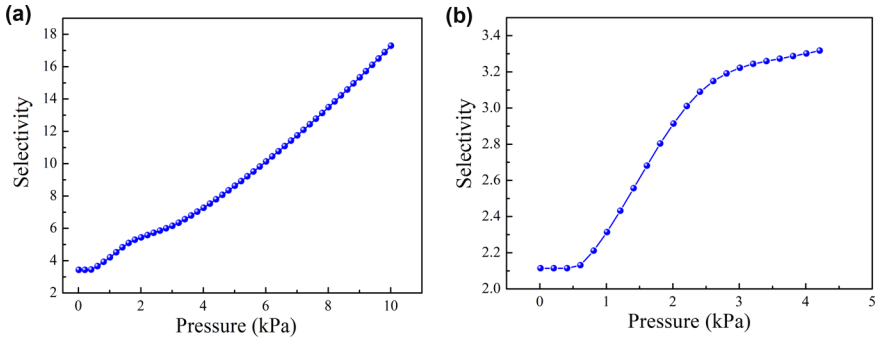

Figure 13. Adsorption selectivity calculated with the IAST method for equimolar binary mixtures of (a) methanol−ethanol and (b) ethanol−water for DMOF ⊃ PNIPAM-**3** at 30 °C.

increasing the pressure, revealing a capillary condensation phenomenon.[16] Figure 12b displays the possible adsorption surface for DMOF which is detected by rolling a probe molecule of helium over the inner surface of DMOF. It reveals that the probe helium atom can be adsorbed around bdc^{2-} ligands on the *ab* plane whilst the space around DABCO ligands along *c* direction is empty because the helium atom would overlap with DABCO ligands. This indicates that the adsorbate molecules, including water, methanol, and ethanol in this study, are first adsorbed around bdc^{2-} ligands on the *ab* plane of DMOF.[48]

In order to simplify the complex interactions between the confined PNIPAM and DMOF, artificial atomic centers were used to mimic the confined polymer PNIPAM chains to block certain areas of the channel from being accessible to adsorbate molecules. The size and shape of the blocked volume is influenced by the size of the artificial atomic centers. The interaction parameter of these centers is made so small as to have no attractive nor repulsive interaction with the adsorbates (ε/KB = 1). As compared to DMOF, the simulated adsorption uptake of the DMOF ⊃ PNIPAM composite for methanol, ethanol, and water decreased drastically from 17.5, 9.7, and 3.5 to 5.8, 2.0, and 0.7 mmol/g, respectively (see Figure 12c). It reveals that the volume of 1D pores of DMOF decreased significantly because of the confined artificial atomic centers, resulting in a reduced space for water, methanol, and ethanol adsorption. Figure 12d confirms that the possible adsorption surface of the DMOF ⊃ PNIPAM composite changed as compared to that of DMOF, in which the probe helium atom can only be present at the top-left part of the 1D pores and on the surface around the confined artificial atomic centers. In order to confirm that the confined PNIPAM decreases the hydrophobicity of DMOF, we gradually increased the attraction (from ε/KB = 1 to 5 and 10 artificial atomic centers) between the artificial atomic centers and adsorbate molecules, including water, methanol, and ethanol. This means that the artificial atomic centers provide stronger affinity for the adsorbate molecules, thus mimicking that the amide groups of PNIPAM have interaction with water, methanol, and ethanol molecules via hydrogen bonding.[39] In the low pressure range, the initial plateaus in DMOF ⊃ PNIPAM composite's water, methanol, and ethanol adsorption isotherms become shorter as the attraction increases (see Figures S8−S10 in Supporting Information). This is reasonable because the stronger affinity that the confined artificial atomic centers have the more polar molecules they can adsorb in the initial pressure range.[30]

Summarizing, the GCMC molecular simulation results indicate that the adsorption space of DMOF can be decreased by incorporating artificial atomic centers in its 1D pores, thus resulting in decreased adsorption uptakes for water, methanol, and ethanol. Increasing the affinity of artificial atomic centers for water, methanol, and ethanol can decrease the hydrophobicity of the DMOF ⊃ PNIPAM composite, thus increasing the adsorption uptakes in the initial pressure range and narrowing the initial plateaus of the adsorption isotherms. These results are in agreement with the experimental adsorption properties of the DMOF and DMOF ⊃ PNIPAM-**3** composite. However, the simulated adsorption properties of the DMOF ⊃ PNIPAM composite do not exactly match the observed experimental adsorption behavior. This means that simulated data do not show a preferential adsorption for water over ethanol. This is likely because of the simplified artificial atomic centers which are still different than the actual complex PNIPAM chains.

3.3. Separation and Regeneration Studies. Based on the adsorption studies discussed above, one may conclude that both the DMOF and DMOF ⊃ PNIPAM-**3** composite are promising candidates for water−ethanol and methanol−ethanol separation processed because both materials have very different adsorption behaviors for water, methanol, and ethanol. However, the pristine DMOF cannot be directly used in water−alcohol separation applications because of its weak stability in the presence of water. The PXRD patterns of DMOF (Figure S11) indicate clearly that the structure of DMOF is completely changed after water adsorption, in agreement with earlier studies.[17,36] By sharp contrast, DMOF ⊃ PNIPAM-**3** retains its crystallinity after water adsorption (see Figure S11 in Supporting Information). This is likely due to the fact that the confined PNIPAM chains facilitate water adsorption on their amide groups, thereby preventing the decomposition of DMOF. Moreover, both DMOF and DMOF ⊃ PNIPAM-**3** retain their structures after methanol and ethanol adsorption, confirming their structure stability in the presence of alcohol molecules (see Figure S12 in Supporting Information). The stability of DMOF in methanol and ethanol adsorption probably is likely because of the preferential occupancy of these molecules within the 1D channels of DMOF without affecting the overall structural topology.[38] DMOF ⊃ PNIPAM-**3** has increased stability also because of the amide groups of confined PNIPAM which provide preferential adsorption sites for methanol and ethanol molecules, thus preventing structural changes.

The ideal adsorbed solution theory (IAST) simulation method was used to evaluate the potential of the DMOF ⊃

DOI: 10.1021/acsami.9b14367
ACS Appl. Mater. Interfaces 2019, 11, 41383−41393

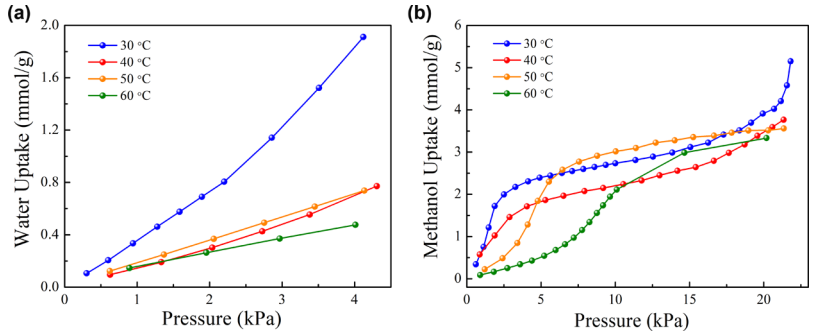

Figure 14. (a) Water adsorption isotherms for the DMOF ⊃ PNIPAM-**3** composite at 30, 40, 50, and 60 °C, respectively. (b) Methanol adsorption isotherms for the DMOF ⊃ PNIPAM-**3** composite at 30, 40, 50, and 60 °C, respectively.

PNIPAM-**3** composite for equimolar water−ethanol and methanol−ethanol separations. As seen in Figure 13, the DMOF ⊃ PNIPAM-**3** composite shows a selective adsorption for methanol and water over ethanol. The selectivity of methanol−ethanol and water−ethanol increased from 3.5 to 17.3 and 2.1 to 3.3 with the increasing of pressure, respectively. An increased adsorption selectivity can be obtained for both methanol−ethanol and water−ethanol equimolar mixtures, mainly because the methanol and water uptake of the DMOF ⊃ PNIPAM-**3** composite increases faster than ethanol uptake.[49] Selectivities calculated with the IAST method using equimolar water−alcohol mixtures have been reported for both MOFs and MOF-based composites. Thus, DMOF ⊃ PNIPAM-**3** in this study has a higher methanol−ethanol selectivity than ZIF-8@TSO (up to 3.8),[50] ZIF-8 (up to 4.5),[50] TetZB (up to ∼1)[13] and $[Cu_2(tpt)_2(CH_3CN)_2](BF_4)_2$ (up to 11).[51] It also has a higher water−ethanol selectivity as compared with ZIF-8@TSO (up to 1.8).[50] The water−ethanol selectivity is lower as compared with ZIF-8 and TetZB as a result of the high hydrophobicity of these frameworks. $[Cu_2(tpt)_2(CH_3CN)_2](BF_4)_2$ has a unique molecular length-selective effect which favors selective water adsorption.[13,50,51]

So far, not too many studies focus on the regeneration of MOFs when they are applied in adsorptive separations.[52−55] As discussed above, a unique feature of the PNIPAM is that it can undergo a phase transition from hydrophilic to hydrophobic and vice versa when it faces an outer temperature change.[23,24] Such feature makes the DMOF ⊃ PNIPAM composites interesting candidates for studying adsorption−desorption processes. Therefore, subsequent studies aimed at studying the water and methanol desorption processes by tuning the hydrophilic−hydrophobic behavior of the DMOF ⊃ PNIPAM-**3** composite as a function of temperature. Figure 14a shows that the water uptake of DMOF ⊃ PNIPAM-**3** at 4 kPa decreased by increasing the temperature. At 60 °C, the isotherm is linear over the entire pressure range (0−4 kPa) with a very low uptake (<0.4 mmol/g). It indicates that the interaction between DMOF ⊃ PNIPAM-**3** and water is very weak and the composite becomes hydrophobic. The decreased water adsorption uptakes of the DMOF ⊃ PNIPAM-**3** composite by increasing temperature suggest that the hydrophobicity of the composite increased. This is because the amide groups of the confined PNIPAM form hydrogen bonds of N−H···O type with adsorbed water molecules at low temperature, while the hydrogen bonding breaks gradually and inner N−H···O═C hydrogen bonds between adjacent amide groups of PNIPAM chains are formed when the temperature increases.[56]

Figure 14b shows DMOF ⊃ PNIPAM-**3** composite's methanol adsorption isotherms as a function of temperature. It is observed that the initial plateau of the methanol adsorption isotherms is gradually extended by increasing the temperature. Such behavior confirms that the DMOF ⊃ PNIPAM-**3** composite becomes hydrophobic at higher temperatures, thus the weak interactions between the composite and methanol lead to lower methanol uptake in the initial pressure range. This is also because of the intermolecular hydrogen bonds which are gradually replaced by intramolecular hydrogen bonds, similar to composite's water adsorption.[56] However, different than the water uptake, which decreases significantly by increasing the temperature, the methanol uptake of DMOF ⊃ PNIPAM-**3** decreased only little. This can be explained by the fact that methanol molecules tend to accumulate within the pores of the composite through capillary condensation by increasing the methanol pressure.

The hydrophobic feature of the DMOF ⊃ PNIPAM-**3** composite above 60 °C inspired us to regenerate it by desorbing the adsorbed water and methanol molecules at this temperature. Therefore, the DMOF ⊃ PNIPAM-**3** composite is regenerated at 60 °C and three consecutive adsorption−regeneration cycles for both water and methanol have been obtained (see Figures S13 and S14 in Supporting Information). The adsorption uptake of each cycle is similar to each other; however, a small difference in isotherms can be observed, probably because of the movement of PNIPAM chains within 1D pores of DMOF after each cycle. Notably, this regeneration temperature of the DMOF ⊃ PNIPAM-**3** composite is lower than that of some other porous adsorbents used in similar applications, such as DMOF itself (70−80 °C for desorbing methanol and ethanol),[16] Linda Type 4A molecular sieves (200−300 °C for desorbing water),[16] UiO-66 and H_2N-MIL-125 (120 °C for desorbing water),[57] and CNT@MIL-68 (Al) (100 °C for desorbing phenol).[58] Such a lower regeneration energy makes the DMOF ⊃ PNIPAM-**3** composite a more suitable adsorbent for the water−alcohol adsorptive separations.

4. CONCLUSIONS

MOFs-based composites of type DMOF ⊃ PNIPAM were synthesized using in situ polymerization of NIPAM monomers within the 1D pores of DMOF. As compared to pristine DMOF, the pore size of composites narrowed due to the fact that PNIPAM chains were blocking partially the 1D pores of DMOF. Consequently, the composites' hydrophobicity decreased because the amide groups of the confined PNIPAM have adsorptive affinity for water and alcohols. Additionally,

DOI: 10.1021/acsami.9b14367
ACS Appl. Mater. Interfaces 2019, 11, 41383−41393

the pore size and hydrophobicity of DMOF ⊃ PNIPAM composites can be controlled by adjusting the loading of PNIPAM in the composites. For DMOF ⊃ PNIPAM-**3**, which has the highest loading of PNIPAM, an increased water adsorption uptake and an increased water stability are observed as compared to the pristine DMOF. Both the experimental results and GCMC simulations of DMOF ⊃ PNIPAM-**3** for water and alcohol adsorption reveal that it can adsorb selectively water and methanol over ethanol. The DMOF ⊃ PNIPAM-**3** composite shows a selectivity as high as 17.3 and 3.3 in equimolar methanol−ethanol and water−ethanol mixtures, as indicated by IAST simulations. The regeneration and desorption studies on DMOF ⊃ PNIPAM-**3** show that the adsorbed water and methanol molecules can be removed at 60 °C. At this temperature, the confined PNIPAM chains undergo a transition between hydrophilic and hydrophobic phases in response to the temperature change. This work provided a rational strategy for the design of a water-stable MOF-based composite with adjustable pore sizes and tunable adsorption for water, methanol and ethanol.

■ ASSOCIATED CONTENT

Supporting Information

The Supporting Information is available free of charge on the ACS Publications website at DOI: 10.1021/acsami.9b14367.

FTIR spectra, ^{1}H NMR spectroscopy, elemental analysis, adsorption heat of water and methanol, adsorption simulation, structural stability and regeneration studies (PDF)

■ AUTHOR INFORMATION

Corresponding Author

*E-mail: s.grecea@uva.nl.

ORCID

David Dubbeldam: 0000-0002-4382-1509

Stefania Tanase: 0000-0003-2830-1924

Notes

The authors declare no competing financial interest.

■ ACKNOWLEDGMENTS

Y.T. acknowledges the China Scholarship Council (CSC) for a PhD fellowship. Prof. Wesley R. Browne (University of Groningen) is kindly acknowledged for the Raman spectra. This work is part of the Research Priority Area Sustainable Chemistry of the University of Amsterdam, http://suschem.uva.nl.

■ REFERENCES

(1) Ragauskas, A. J.; Williams, C. K.; Davison, B. H.; Britovsek, G.; Cairney, J.; Eckert, C. A.; Frederick, W. J.; Hallett, J. P.; Leak, D. J.; Liotta, C. L.; Mielenz, J. R.; Murphy, R.; Templer, R.; Tschaplinski, T. The Path Forward for Biofuels and Biomaterials. *Science* **2006**, *311*, 484−489.

(2) Luque, R.; Herrero-Davila, L.; Campelo, J. M.; Clark, J. H.; Hidalgo, J. M.; Luna, D.; Marinas, J. M.; Romero, A. A. Biofuels: a Technological Perspective. *Energy Environ. Sci.* **2008**, *1*, 542−564.

(3) Sun, J.-K.; Ji, M.; Chen, C.; Wang, W.-G.; Wang, P.; Chen, R.-P.; Zhang, J. A Charge-Polarized Porous Metal-Organic Framework for Gas Chromatographic Separation of Alcohols from Water. *Chem. Commun.* **2013**, *49*, 1624−1626.

(4) Zhang, K.; Lively, R. P.; Zhang, C.; Koros, W. J.; Chance, R. R. Investigating the Intrinsic Ethanol/Water Separation Capability of ZIF-8: an Adsorption and Diffusion Study. *J. Phys. Chem. C* **2013**, *117*, 7214−7225.

(5) Gutiérrez-Sevillano, J. J.; Dubbeldam, D.; Bellarosa, L.; López, N.; Liu, X.; Vlugt, T. J. H.; Calero, S. Strategies to Simultaneously Enhance the Hydrostability and the Alcohol−Water Separation Behavior of Cu-BTC. *J. Phys. Chem. C* **2013**, *117*, 20706−20714.

(6) Rezaei, F.; Webley, P. Structured Adsorbents in Gas Separation Processes. *Sep. Purif. Technol.* **2010**, *70*, 243−256.

(7) Zhao, X.; Wang, Y.; Li, D.-S.; Bu, X.; Feng, P. Metal−Organic Frameworks for Separation. *Adv. Mater.* **2018**, *30*, 1705189.

(8) Chang, Z.; Yang, D.-H.; Xu, J.; Hu, T.-L.; Bu, X.-H. Flexible Metal-Organic Frameworks: Recent Advances and Potential Applications. *Adv. Mater.* **2015**, *27*, 5432−5441.

(9) Lin, R.-B.; Xiang, S.; Xing, H.; Zhou, W.; Chen, B. Exploration of Porous Metal-Organic Frameworks for Gas Separation and Purification. *Coord. Chem. Rev.* **2019**, *378*, 87−103.

(10) Zhang, Q.; Cui, Y.; Qian, G. Goal-Directed Design of Metal-Organic Frameworks for Liquid-Phase Adsorption and Separation. *Coord. Chem. Rev.* **2019**, *378*, 310−332.

(11) Zhang, K.; Lively, R. P.; Dose, M. E.; Brown, A. J.; Zhang, C.; Chung, J.; Nair, S.; Koros, W. J.; Chance, R. R. Alcohol and Water Adsorption in Zeolitic Imidazolate Frameworks. *Chem. Commun.* **2013**, *49*, 3245−3247.

(12) Shigematsu, A.; Yamada, T.; Kitagawa, H. Selective Separation of Water, Methanol, and Ethanol by a Porous Coordination Polymer Built with a Flexible Tetrahedral Ligand. *J. Am. Chem. Soc.* **2012**, *134*, 13145−13147.

(13) Motkuri, R. K.; Thallapally, P. K.; Annapureddy, H. V. R.; Dang, L. X.; Krishna, R.; Nune, S. K.; Fernandez, C. A.; Liu, J.; Mcgrail, B. P. Separation of Polar Compounds Using a Flexible Metal-Organic Framework. *Chem. Commun.* **2015**, *51*, 8421−8424.

(14) Liu, T.-F.; Lü, J.; Lin, X.; Cao, R. Construction of a trigonal bipyramidal cage-based metal−organic framework with hydrophilic pore surface via flexible tetrapodal ligands. *Chem. Commun.* **2010**, *46*, 8439−8441.

(15) Li, J.-R.; Kuppler, R. J.; Zhou, H.-C. Selective Gas Adsorption and Separation in Metal-Organic Frameworks. *Chem. Soc. Rev.* **2009**, *38*, 1477−1504.

(16) Lee, J. Y.; Olson, D. H.; Pan, L.; Emge, T. J.; Li, J. Microporous Metal-Organic Frameworks with High Gas Sorption and Separation Capacity. *Adv. Funct. Mater.* **2007**, *17*, 1255−1262.

(17) Schoenecker, P. M.; Carson, C. G.; Jasuja, H.; Flemming, C. J. J.; Walton, K. S. Effect of Water Adsorption on Retention of Structure and Surface Area of Metal-Organic Frameworks. *Ind. Eng. Chem. Res.* **2012**, *51*, 6513−6519.

(18) Dybtsev, D. N.; Chun, H.; Kim, K. Rigid and Flexible: A Highly Porous Metal-Organic Framework with Unusual Guest-Dependent Dynamic Behavior. *Angew. Chem., Int. Ed.* **2004**, *43*, 5033−5036.

(19) Distefano, G.; Suzuki, H.; Tsujimoto, M.; Isoda, S.; Bracco, S.; Comotti, A.; Sozzani, P.; Uemura, T.; Kitagawa, S. Highly Ordered Alignment of a Vinyl Polymer by Host-Guest Cross-Polymerization. *Nat. Chem.* **2013**, *5*, 335−341.

(20) Yanai, N.; Uemura, T.; Kitagawa, S. Behavior of Binary Guests in a Porous Coordination Polymer. *Chem. Mater.* **2012**, *24*, 4744−4749.

(21) Kitao, T.; Bracco, S.; Comotti, A.; Sozzani, P.; Naito, M.; Seki, S.; Uemura, T.; Kitagawa, S. Confinement of Single Polysilane Chains in Coordination Nanospaces. *J. Am. Chem. Soc.* **2015**, *137*, 5231−5238.

(22) Kitao, T.; Zhang, Y.; Kitagawa, S.; Wang, B.; Uemura, T. Hybridization of MOFs and Polymers. *Chem. Soc. Rev.* **2017**, *46*, 3108−3133.

(23) Jadhav, S. A.; Brunella, V.; Miletto, I.; Berlier, G.; Scalarone, D. Synthesis of Poly(*N*-isopropylacrylamide) by Distillation Precipitation Polymerization and Quantitative Grafting on Mesoporous Silica. *J. Appl. Polym. Sci.* **2016**, *133*, 44181.

(24) Nagata, S.; Kokado, K.; Sada, K. Metal−organic framework tethering PNIPAM for ON−OFF controlled release in solution. *Chem. Commun.* **2015**, *51*, 8614−8617.

(25) Ding, N.; Li, H.; Feng, X.; Wang, Q.; Wang, S.; Ma, L.; Zhou, J.; Wang, B. Partitioning MOF-5 into Confined and Hydrophobic Compartments for Carbon Capture under Humid Conditions. *J. Am. Chem. Soc.* **2016**, *138*, 10100−10103.
(26) Ferreira, A. F. P.; Mittelmeijer-Hazeleger, M. C.; Granato, M. A.; Martins, V. F. D.; Rodrigues, A. E.; Rothenberg, G. Sieving Di-branched from Mono-branched and Linear Alkanes Using ZIF-8: Experimental Proof and Theoretical Explanation. *Phys. Chem. Chem. Phys.* **2013**, *15*, 8795−8804.
(27) Guerrero-Medina, J.; Mass-González, G.; Pacheco-Londoño, L.; Hernández-Rivera, S. P.; Fu, R.; Hernández-Maldonado, A. J. Long and Local Range Structural Changes in M[(bdc)(ted)0.5] (M = Zn, Ni or Cu) Metal Organic Frameworks upon Spontaneous Thermal Dispersion of LiCl and Adsorption of Carbon Dioxide. *Microporous Mesoporous Mater.* **2015**, *212*, 8−17.
(28) Nabipour, H.; Soltani, B.; Ahmadi Nasab, N. Gentamicin Loaded $Zn_2(bdc)_2(dabco)$ Frameworks as Efficient Materials for Drug Delivery and Antibacterial Activity. *J. Inorg. Organomet. Polym. Mater.* **2018**, *28*, 1206−1213.
(29) Shi, S.; Zhang, L.; Wang, T.; Wang, Q.; Gao, Y.; Wang, N. Poly(*N*-isopropylacrylamide)−Au hybrid microgels: synthesis, characterization, thermally tunable optical and catalytic properties. *Soft Matter* **2013**, *9*, 10966−10970.
(30) Tan, K.; Nijem, N.; Gao, Y.; Zuluaga, S.; Li, J.; Thonhauser, T.; Chabal, Y. J. Water Interactions in Metal Organic Frameworks. *CrystEngComm* **2015**, *17*, 247−260.
(31) Sanz, B.; von Bilderling, C.; Tuninetti, J. S.; Pietrasanta, L.; Mijangos, C.; Longo, G. S.; Azzaroni, O.; Giussi, J. M. Thermally-induced Softening of PNIPAM-based Nanopillar Arrays. *Soft Matter* **2017**, *13*, 2453−2464.
(32) Sun, S.; Wu, P. Tailoring the Morphology of Branched Poly(N-isopropylacrylamide) *via* Self-condensing Atom-transfer Radical Copolymerization and Its Unique Self-assembly Behavior in Alcohol. *Soft Matter* **2011**, *7*, 7526−7531.
(33) Dhumure, A. B.; Patil, A. B.; Kulkarni, A. S.; Voevodina, I.; Scandola, M.; Shinde, V. S. Thermoresponsive copolymers with pendant D-galactosyl 1,2,3-triazole groups: synthesis, characterization and thermal behavior. *New J. Chem.* **2015**, *39*, 8179−8187.
(34) Uemura, T.; Horike, S.; Kitagawa, K.; Mizuno, M.; Endo, K.; Bracco, S.; Comotti, A.; Sozzani, P.; Nagaoka, M.; Kitagawa, S. Conformation and Molecular Dynamics of Single Polystyrene Chain Confined in Coordination Nanospace. *J. Am. Chem. Soc.* **2008**, *130*, 6781−6788.
(35) Ji, X.; Hampsey, J. E.; Hu, Q.; He, J.; Yang, Z.; Lu, Y. Mesoporous Silica-reinforced Polymer Nanocomposites. *Chem. Mater.* **2003**, *15*, 3656−3662.
(36) Jasuja, H.; Burtch, N. C.; Huang, Y.-G.; Cai, Y.; Walton, K. S. Kinetic Water Stability of an Isostructural Family of Zinc-based Pillared Metal-Organic Frameworks. *Langmuir* **2013**, *29*, 633−642.
(37) Nalaparaju, A.; Zhao, X. S.; Jiang, J. W. Molecular Understanding for the Adsorption of Water and Alcohols in Hydrophilic and Hydrophobic Zeolitic Metal−Organic Frameworks. *J. Phys. Chem. C* **2010**, *114*, 11542−11550.
(38) Chen, Y. F.; Lee, J. Y.; Babarao, R.; Li, J.; Jiang, J. W. A Highly Hydrophobic Metal-Organic Framework $Zn(BDC)(TED)_{0.5}$ for Adsorption and Separation of CH_3OH/H_2O and CO_2/CH_4: An Integrated Experimental and Simulation Study. *J. Phys. Chem. C* **2010**, *114*, 6602−6609.
(39) Hasegawa, S.; Horike, S.; Matsuda, R.; Furukawa, S.; Mochizuki, K.; Kinoshita, Y.; Kitagawa, S. Three-dimensional Porous Coordination Polymer Functionalized with Amide Groups Based on Tridentate Ligand: Selective Sorption and Catalysis. *J. Am. Chem. Soc.* **2007**, *129*, 2607−2614.
(40) Khutia, A.; Rammelberg, H. U.; Schmidt, T.; Henninger, S.; Janiak, C. Water Sorption Cycle Measurements on Functionalized MIL-101Cr for Heat Transformation Application. *Chem. Mater.* **2013**, *25*, 790−798.
(41) Jeremias, F.; Khutia, A.; Henninger, S. K.; Janiak, C. MIL-100(Al, Fe) as water adsorbents for heat transformation purposes-a promising application. *J. Mater. Chem.* **2012**, *22*, 10148−10151.
(42) Jeremias, F.; Lozan, V.; Henninger, S. K.; Janiak, C. Programming MOFs for Water Sorption: Amino-functionalized MIL-125 and UiO-66 for Heat Transformation and Heat Storage Applications. *Dalton Trans.* **2013**, *42*, 15967−15973.
(43) de Lange, M. F.; Verouden, K. J. F. M.; Vlugt, T. J. H.; Gascon, J.; Kapteijn, F. Adsorption-Driven Heat Pumps: The Potential of Metal-Organic Frameworks. *Chem. Rev.* **2015**, *115*, 12205−12250.
(44) Küsgens, P.; Rose, M.; Senkovska, I.; Fröde, H.; Henschel, A.; Siegle, S.; Kaskel, S. Characterization of Metal-Organic Frameworks by Water Adsorption. *Microporous Mesoporous Mater.* **2009**, *120*, 325−330.
(45) Kaneko, K.; Hanzawa, Y.; Iiyama, T.; Kanda, T.; Suzuki, T. Cluster-Mediated Water Adsorption on Carbon Nanopores. *Adsorption* **1999**, *5*, 7−13.
(46) Dubbeldam, D.; Calero, S.; Ellis, D. E.; Snurr, R. Q. RASPA: Molecular Simulation Software for Adsorption and Diffusion in Flexible Nanoporous Materials. *Mol. Simul.* **2016**, *42*, 81−101.
(47) Wang, H.-J.; Xi, X.-K.; Kleinhammes, A.; Wu, Y. Temperature-induced Hydrophobic-hydrophilic Transition Observed by Water Adsorption. *Science* **2008**, *322*, 80−83.
(48) Liang, Z.; Marshall, M.; Chaffee, A. L. CO_2 adsorption, selectivity and water tolerance of pillared-layer metal organic frameworks. *Microporous Mesoporous Mater.* **2010**, *132*, 305−310.
(49) Challa, S. R.; Sholl, D. S.; Johnson, J. K. Adsorption and Separation of Hydrogen Isotopes in Carbon Nanotubes: Multi-component Grand Canonical Monte Carlo Simulations. *J. Chem. Phys.* **2002**, *116*, 814−824.
(50) Tang, Y.; Dubbeldam, D.; Guo, X.; Rothenberg, G.; Tanase, S. Efficient Separation of Ethanol-Methanol and Ethanol-Water Mixtures Using ZIF-8 Supported on a Hierarchical Porous Mixed-Oxide Substrate. *ACS Appl. Mater. Interfaces* **2019**, *11*, 21126−21136.
(51) Kondo, A.; Yashiro, T.; Okada, N.; Hiraide, S.; Ohkubo, T.; Tanaka, H.; Maeda, K. Selective Molecular-Gating Adsorption in a Novel Copper-Based Metal-Organic Framework. *J. Mater. Chem. A* **2018**, *6*, 5910−5918.
(52) Khaletskaya, K.; Reboul, J.; Meilikhov, M.; Nakahama, M.; Diring, S.; Tsujimoto, M.; Isoda, S.; Kim, F.; Kamei, K.-i.; Fischer, R. A.; Kitagawa, S.; Furukawa, S. Integration of Porous Coordination Polymers and Gold Nanorods into Core−Shell Mesoscopic Composites toward Light-Induced Molecular Release. *J. Am. Chem. Soc.* **2013**, *135*, 10998−11005.
(53) Ye, S.; Jiang, X.; Ruan, L.-W.; Liu, B.; Wang, Y.-M.; Zhu, J.-F.; Qiu, L.-G. Post-combustion CO_2 Capture with the HKUST-1 and MIL-101 (Cr) Metal−Organic Frameworks: Adsorption, Separation and Regeneration Investigations. *Microporous Mesoporous Mater.* **2013**, *179*, 191−197.
(54) Begum, S.; Horike, S.; Kitagawa, S.; Krautscheid, H. Water Stable Triazolyl Phosphonate MOFs: Steep Water Uptake and Facile Regeneration. *Dalton Trans.* **2015**, *44*, 18727−18730.
(55) Blanco-Brieva, G.; Campos-Martin, J. M.; Al-Zahrani, S. M.; Fierro, J. L. G. Thermal Regeneration of the Metal Organic Frameworks Used in the Adsorption of Refractory Organosulfur Compounds from Liquid Fuels. *Fuel* **2013**, *105*, 459−465.
(56) Cheng, H.; Shen, L.; Wu, C. LLS and FTIR Studies on the Hysteresis in Association and Dissociation of Poly(*N*-isopropylacrylamide) Chains in Water. *Macromolecules* **2006**, *39*, 2325−2329.
(57) Jeremias, F.; Lozan, V.; Henninger, S. K.; Janiak, C. Programming MOFs for Water Sorption: Amino-Functionalized MIL-125 and UiO-66 for Heat Transformation and Heat Storage Applications. *Dalton Trans.* **2013**, *42*, 15967−15973.
(58) Han, T.; Xiao, Y.; Tong, M.; Huang, H.; Liu, D.; Wang, L.; Zhong, C. Synthesis of CNT@MIL-68(Al) composites with improved adsorption capacity for phenol in aqueous solution. *Chem. Eng. J.* **2015**, *275*, 134−141.

DOI: 10.1021/acsami.9b14367
ACS Appl. Mater. Interfaces 2019, 11, 41383−41393